Electronic interactions in the organic conductors $(TMTSF)_2X$ (X =ClO_4 and PF_6) and $(TMTTF)_2X$ (X =Br and PF_6) from their infrared spectra

Danilo Pedron, Renato Bozio, Moreno Meneghetti, and Cesare Pecile
Department of Physical Chemistry, University of Padova, 2 Via Loredan, I-35131 Padova, Italy
(Received 11 October 1993; revised manuscript received 14 January 1994)

Accurate measurements of the polarized reflectance spectra of the series of isostructural organic conductors $(TMTSF)_2ClO_4$, $(TMTSF)_2PF_6$, $(TMTTF)_2Br$, and $(TMTSF)_2PF_6$ (where TMTSF denotes tetramethyltetraselenafulvalane and TMTTF denotes tetramethyltetrathiafulvalene) at room temperature are reported. A dimerized molecular chain model is used to analyze these spectra as well as those previously reported [C. C. Homes and J. E. Eldridge, Phys. Rev. B **42**, 9522 (1990); J. E. Eldridge and C. C. Homes, *ibid.* **43**, 13 971 (1991)] for $(TMTSF)_2BF_4$ and $(TMTSF)_2ReO_4$ and the corresponding conductivity spectra obtained by Kramers-Kronig transformation. The complex structures observed in the spectra are successfully accounted for by assuming that the double occupancy of the band states is effectively excluded so that the Fermi level lies inside a narrow gap induced in these materials by a small dimerization of the molecular stacks. The spectral changes observed among different members of the series are reproduced by varying a limited number of model parameters in a way that follows closely the known changes of the crystal structural properties. Fitting of the experimental data enables us to estimate the parameters of the band structure, namely the transfer integral and the dimerization gap amplitude. Use of self-consistent relations inherent in the adopted model allows us to conclude that a static potential rather than a Peierls-type phonon-induced mechanism plays the dominant role in driving the formation of charge-density waves and the opening of the gap. The same model analysis accounts for the presence of vibronic structures induced by the coupling of the conduction electrons with intramolecular vibrational modes of TMTSF or TMTTF. It has been thereby possible to evaluate the coupling constants for the individual vibrational modes with a greater degree of reliability than in previous attempts. The general physical picture of the studied materials at room temperature as narrow-gap correlated semiconductors is briefly discussed.

I. INTRODUCTION

The rapid evolution of the field of organic molecular conductors[1–4] has gone through two distinguishable successive stages. At first, the interest was mainly focused on highly one–dimensional (1D), electronically incommensurate materials such as tetrathiafulvalene-tetracyanoquinodimethane (TTF-TCNQ) and the TTF mixed-valence halides. These crystals are characterized by very weak interactions between the molecular chains (or stacks) making up their structures and by an average number of carriers per molecule which cannot be expressed by a simple rational number (the Fermi wave vector is thus incommensurate with the reciprocal lattice vectors). They exhibit an intrinsic instability of the metallic state towards a Peierls-type metal-insulator (M-I) transition[5] that prevents the observation of superconductivity. In this respect, the discovery[6] of superconducting transitions in the radical cation salts of TMTSF (where TMTSF denotes tetramethyltetraselenafulvalene), known as the Bechgaard salts, represented a turning point. Compared to previously known materials, two differences are readily recognizable in the Bechgaard salts. Their chemical formula, $(TMTSF)_2X$ with X an inorganic closed-shell anion, directly implies a carrier density of half a hole per molecule, and thus a commensurate electronic structure. In a one-electron tight-binding scheme these materials would be quarter-filled band systems. Furthermore, there is evidence[3] that at low temperature and under an applied pressure the behavior of the Bechgaard salts is closer to highly anisotropic two dimensional (2D) than to quasi-1D. The enhanced stability of the metallic state and the absence of Peierls-type transitions is most likely attributable to the increased dimensionality of the electronic structure.

Since the discovery of the Bechgaard salts a great deal of research activity has been focusing on radical ion salts with 2:1 stoichiometry and with relevant interstack interactions up to the point that the electronic bands become almost isotropically 2D with closed Fermi surfaces. This is the case of, e.g., the $(BEDT\text{–}TTF)_2X$ (where BEDT-TTF denotes bis(ethylenedithio)tetrathiafulvalene) salts as well as other cation radical salts of TTF derivatives.[3] More recently, the anion radical salt $Cu(DM\text{-}DCNQI)_2$ (where DM-DCNQI denotes 2,5-dimethyl-N,N'-dicyanoquinonediimine) and its analogs have been shown to possess a quasi-2D structure and a metallic state stable down to very low temperature.[1] With respect to these systems, the Bechgaard salts may be thought to represent a bridge between 1D and 2D materials, particularly if one considers also their sulfur analogs $(TMTTF)_2X$ (where TMTTF denotes tetramethyltetrathiafulvalene). In fact, on the one hand, $(TMTTF)_2PF_6$ undergoes a spin-Peierls transition, that is a clear signature of 1D behavior, and on the other hand

$(TMTTF)_2Br$ under moderate pressure exhibits a stable metallic state and possibly a superconducting transition.

Spectroscopic studies, especially in the near- to far-infrared part of the spectrum, have proved to be one of the most effective tools for gaining information on the structural, electronic, and phase transition properties of organic molecular conductors.[7] Experimental estimates of the important electronic interactions can be obtained by analyzing specific features of the spectra. For instance, the electronic bandwidth can be evaluated from a Drude fitting of the plasma edge in reflectance spectra, the presence of narrow gaps or pseudogaps can be monitored from the far-infrared conductivity, the electron-phonon coupling constants can be obtained from the vibronic structures observed in the semiconducting phases. The role of direct electron-electron correlations can be assessed by searching for the possible presence of charge transfer (CT) bands[8] or by comparison of the measured oscillator strength with theoretical estimates of the optical sum rule for independent electrons.[9] It is worth noting that, as shown theoretically, the on-site electron correlation (U) of the Hubbard model[10,11] may play a particularly important role in quarter-filled band systems such as the 2:1 salts.[12]

In the past few years we have proposed an approach to the analysis of optical data pertaining to 1D quarter-filled systems whereby all the important features of the spectra carrying relevant information on the electronic structure and interactions can be analyzed by the use of a single theoretical model.[13–18,7] Such a model[14] is clearly oversimplified if compared with the very complicated structure of real organic molecular conductors, yet it contains enough features to allow one to model the interplay of some of the most important interactions. The main limitation is found in dealing properly with electron correlations. As is well known, this is as yet an unsolved problem, particularly if one is interested in correlation functions and optical properties[19] of an ideally infinite system. With respect to this problem, the only degree of freedom we have with our model is either to treat the charge carriers as ordinary electrons (or holes) or to consider them as spinless particles. The two schemes would correspond to the limits of no correlation or of infinite on-site repulsion U in a simple Hubbard model.[20]

As a first application of our approach we have compared stack-axis-polarized conductivity spectra measured at room temperature for $(TMTTF)_2PF_6$, $(TMTTF)_2Br$, and $(TMTSF)_2PF_6$ with calculations carried out according to the two schemes.[15] The large-U limit proved to be clearly superior for the first salt. However, a similar conclusion for the other two materials could not be safely drawn in view of the limitations of the model used and of uncertainties in the accuracy of the experimental data. In particular, the large-U calculations did not account for the contributions to the optical functions of intraband transitions involving charge carriers thermally excited across a narrow dimerization gap. In calculations presented in a later work[16] we have included the above feature as well as the ability to account for the coupling of electrons to many intramolecular modes. One additional important modification to be discussed below has also allowed us to get insights into the origin of the gap. Comparison was then made with room-temperature polarized reflectance and conductivity spectra of $(TMTSF)_2ClO_4$, a material which is considered to be representative of the Bechgaard salts with *metallic* behavior. It was suggested that the large-U limit applies also to the TMTSF salts with comparatively large room-temperature dc conductivity.[17,18] On account of the small stack dimerization, this implies that at room temperature they should be regarded as strongly correlated semiconductors with very narrow gaps. The gap amplitude is largely determined by the interaction with static potentials rather than by a Peierls mechanism.

The present work aims at putting on firmer experimental grounds the conclusions previously suggested on the basis of preliminary results. This is achieved by improving and extending the experimental data and their analysis. In particular, we have measured accurate polarized reflectance data for a series of $(TMTSF)_2X$ and $(TMTTF)_2X$ salts whose room-temperature structures are known and exhibit a smooth variation of some relevant crystallographic parameters. On the one hand, this enables one to check the scaling of the electronic and optical properties with the smoothly varying structural ones. On the other hand, it allows us to be confident in extending our conclusions to materials with very small amplitude of the stack dimerization and of the semiconducting gap.

In Sec. II we give some details of the materials preparation, of the instrumentation and procedures used for measuring reflectance spectra, and of the methods adopted for the data reduction. The specular reflectance spectra (15–9000 cm^{-1}) polarized parallel to the stacking axis measured at room temperature are reported in Sec. III. The infrared conductivity spectra obtained by Kramers–Kronig transformation[21] of the above data as well as of room-temperature reflectance spectra recently reported[22,23] for $(TMTSF)_2BF_4$ and $(TMTSF)_2ReO_4$ are also given. An outline of the theoretical model used in analyzing the experimental data is provided in Sec. IV followed by the presentation of the results of the model fitting of the data. In Sec. V we discuss the parameters obtained and propose a general picture of the physical properties of the Bechgaard salts at high temperature based on our optical studies. A summary and some final remarks are given in Sec. VI.

II. EXPERIMENT

TMTSF and TMTTF were synthesized and purified as previously reported.[24] Single crystals of the studied compounds have been prepared by the standard electrocrystallization method.[25] The crystals grow mainly along the stacking **a** direction and have a needle-shaped habit. They have typical dimensions of 4–8 mm along the **a** axis and 0.2–0.4 mm along the transverse directions. The crystals are dark colored and have good specular surfaces with a high metalliclike reflectivity. Samples suitable for polarized reflectance measurements with typical dimensions of 2–4 mm^2 have been obtained as mosaics of 2–4 optically aligned crystals.

For $(TMTTF)_2PF_6$, $(TMTTF)_2Br$, $(TMTSF)_2PF_6$, and $(TMTSF)_2ClO_4$, we have measured the room-temperature reflectance spectra $R(\omega)$ in the region 10–10 000 cm^{-1} with radiation at near-normal incidence polarized along the stacking direction. The instrumentation used for the measurements consisted of a Fourier transform infrared spectrometer (Bruker IFS 113v) equipped with a specular reflectance insert having an incidence angle of about 10°. An InSb photovoltaic cell, an MCT photoconductor, and a Ga-doped Ge bolometer were used as detectors in the near-, mid-, and far-infrared regions, respectively. Spectral resolutions of 2 cm^{-1} in the far- and midinfrared and 4 cm^{-1} in the near-infrared were adopted.

The high reflectivity of the studied materials in the far- and midinfrared requires a great accuracy in the measurements. In fact, for the $(TMTSF)_2PF_6$ and $(TMTSF)_2ClO_4$ salts in the spectral region from 10 to 4000 cm^{-1}, $R(\omega)$ is always greater than 0.8. This implies that the spectral information about the optical functions is contained in the less than 20% deviation from 1.0 of the reflectance. It is clear that, in order to obtain significant data, the measurements must be done with an accuracy of a few percent. Owing to the irregular and discontinuous reflecting surfaces of the mosaic samples and to the single-beam measurement technique, this has required the adoption of a complex normalization procedure for the reflectance data. For every sample and in all the spectral regions the measured reflectance spectrum has been obtained as the ratio between the power reflected from the mosaic surface and that reflected from the mosaic itself coated with a thin layer of evaporated gold. The gold layer is considered as an ideal reflector that however accounts for the natural discontinuities of the mosaic surface. To correct for the instrumental fluctuations, the resulting spectrum has also been multiplied by the inverse ratio of two reflectance spectra measured from a flat aluminum mirror before and after the gold deposition. The mirror was mounted at the side of the mosaic on the same holder anchored to an X-Y positioning system. This allows the alternate positioning of the sample and of the reference mirror on the focus of the incident beam in a reproducible way.

Infrared conductivity spectra $\sigma(\omega)$ have been obtained through a Kramers-Kronig transformation of the reflectance data.[21] This requires an integration over the full frequency axis from zero to infinity that is achieved as follows. We have extended the reflectance spectra to the visible and ultraviolet region with literature data. In particular, for the TMTSF compounds we have used the data on $(TMTSF)_2ClO_4$ from Refs. 26 and 27, for the TMTTF compounds the data on $(TMTTF)_2PF_6$ from Ref. 28, and those on $(TMTTF)_2IO_3$ from Ref. 29. For frequencies above the ultraviolet region we have imposed on $R(\omega)$ an ω^{-4} dependence that is typical of free electrons.[21] In the low-frequency limit we have extrapolated $R(\omega)$ to zero frequency with a Hagen-Reubens[30] behavior

$$R(\omega) = 1 - (2\omega/\pi\sigma_{dc})^{-1/2}. \quad (1)$$

This is typical of ordinary metals and appears to be suitable to account for the finite room-temperature dc conductivity σ_{dc} of the materials considered. In Eq. (1), σ_{dc} is chosen in order to match the low-frequency limit of the measured reflectance.

III. RESULTS

Figure 1 (a)–(d) reports the reflectance spectra (15–9000 cm^{-1}) of $(TMTSF)_2ClO_4$, $(TMTSF)_2PF_6$, $(TMTTF)_2Br$, and $(TMTTF)_2PF_6$ measured at room temperature with the electric vector of the linearly polarized incident radiation parallel to the stacking **a** axis. For the last three compounds, our spectra compare rather well with those already reported by Jacobsen *et al.*[28] particularly for what concerns the most prominent spectral changes observed on going from one sample to another. However the reflectance values we measured for $(TMTSF)_2PF_6$ and $(TMTTF)_2Br$ in the region below 4000 cm^{-1} are up to 10 % higher than those of Jacobsen *et al.*[28] Furthermore, we observe a shallow minimum in the reflectivity of $(TMTSF)_2PF_6$ between 500 and 2000 cm^{-1} whereas the previously measured room-temperature reflectance decreased monotonically. The peak we measure around 1250 cm^{-1} for $(TMTTF)_2Br$ does not reach the high reflectance value ($R = 0.9$) reported by Jacobsen *et al.*[28] On the other hand, our spectrum of $(TMTTF)_2PF_6$ practically coincides with the previous data. For $(TMTSF)_2ClO_4$ comparison is only possible in the plasma edge region where our data agree with those published by Kikuchi *et al.*[26]

A common feature of the measured spectra is a comparatively large value of the reflectance in the far- to midinfrared with a rapid drop to values of a few per-

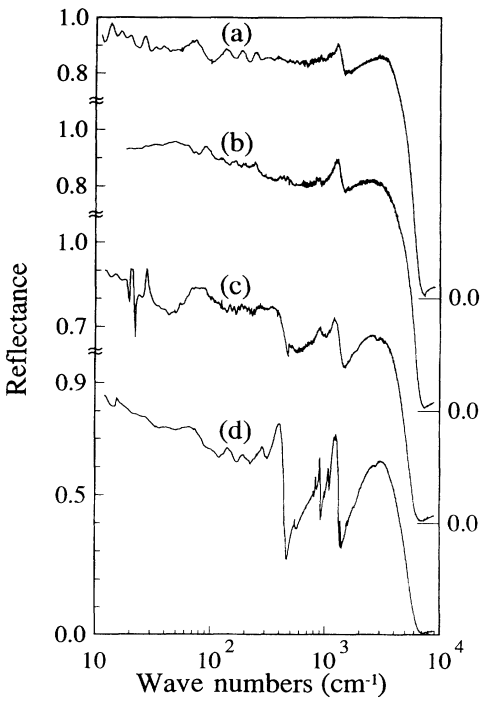

FIG. 1. **E**||**a** polarized infrared reflectance spectra of (a) $(TMTSF)_2ClO_4$; (b) $(TMTSF)_2PF_6$; (c) $(TMTTF)_2Br$; (d) $(TMTTF)_2PF_6$ at room temperature. Note the logarithmic frequency scale.

cent around 7000 cm^{-1}. Superimposed on the high-reflectance region there are narrow peaks of varying amplitude at frequencies typical of molecular vibrations. In agreement with the dc conducting nature of the materials at room temperature, the reflectance value tends to unity as the frequency approaches zero. As previously noted,[28] the reflectance levels in the midinfrared parallel the increase in dc conductivity in the order $(TMTTF)_2PF_6$ < $(TMTTF)_2Br$ < $(TMTSF)_2PF_6$ < $(TMTSF)_2ClO_4$. This implies that the $R = 1$ limit at zero frequency is reached with a smaller slope in the more conducting materials in agreement with the Hagen-Reubens relation, Eq. (1). Other changes observed when comparing the spectra in the order of increasing conductivity of the materials are a decreasing depth of the broad reflectance minimum in the midinfrared and a decreasing amplitude of the peaks superimposed on this minimum.

Measuring reflectance spectra in the far-infrared region from highly reflecting mosaics of tiny single crystals presents some problems originating from diffraction effects. In fact, below a typical frequency of 100 cm^{-1}, when the wavelength of the incident radiation becomes comparable to the transverse dimensions of the needle-shaped crystals, the sample itself acts as a small grating that diffracts the far-infrared radiation. As a result spurious effects may appear in the measured reflectance spectra: (i) modulations of the reflected intensity with narrow frequency periodicities; (ii) a gradual decrease of the reflectance level as the frequency approaches zero. The latter effect has been attributed to a loss of efficiency of the spectrometer optics.[31] Our procedure for obtaining absolute reflectance values by normalization against the reflectance of the gold-coated mosaic allows us to correct for the gradual drift but leaves a residual modulation of the spectra on approaching the low-frequency limit that is observable in the spectra of Fig. 1, notably in that of $(TMTSF)_2ClO_4$ [Fig. 1(a)]. We have verified that this is due to the fact that, although the shape of the modulations is preserved, its amplitude is larger for the gold-coated than for the bare sample. Thus, normalizing the spectra does not completely eliminate the effect.

Kramers–Kronig transformation of the reflectance data of Fig. 1 yields the conductivity spectra shown in Fig. 2 for the spectral range 15–6000 cm^{-1}. The conductivity spectra (c) and (d) of Fig. 2 have been obtained by performing a Kramers-Kronig transformation of the stack-axis-polarized reflectance data of $(TMTSF)_2BF_4$ and $(TMTSF)_2ReO_4$ at room temperature recently reported by Homes and Eldridge.[22,23] This was done in order to make all the conductivity spectra of Fig. 2 directly comparable by using the same extrapolation procedure.

Note that the far-infrared conductivity of $(TMTSF)_2ClO_4$, shown as a dashed curve in Fig. 2(a), has been obtained by averaging the reflectance modulations attributed above to diffraction effects. We have checked that a Kramers-Kronig transformation performed on the raw data yields a modulated conductivity whose average coincides with the data shown in Fig. 2(a). We believe that this procedure, while it certainly washes out any real structure that is present in the spectral region involved, does not affect the general shape of the conductivity spectrum which is crucial in revealing the presence of narrow optical gaps. Support for this view comes from the fact that for $(TMTSF)_2ClO_4$, as well as for the other measured compounds, the far-infrared conductivity extrapolates to a dc value in agreement with direct transport measurements.

As already noted by Jacobsen *et al.*,[28] a most salient feature of the spectra of Fig. 2 is the fact that in all cases they display a conductivity maximum at finite frequency in contrast to the simple Drude behavior of ordinary metals. The conductivity maximum shifts to higher frequencies as the midinfrared reflectance level decreases (Fig. 1) and as the dc conductivity also decreases. This is in itself suggestive of an optical gap and possibly a transport gap of increasing amplitude.

Accompanying the shift to higher frequencies of the conductivity maximum, there is an increase of the amplitude of the midinfrared structures attributed to the coupling of electrons to intramolecular vibrations of the TMTSF and TMTTF units (EMV coupling). Note that the band shapes of these structures change depending on their frequency location relative to the conductivity maximum. They appear as absorptive peaks when their frequency is well below that of the broad maximum, otherwise they display typical Fano antiresonance line shapes.[32] Accounting simultaneously for the shift in frequency of the conductivity maximum and the increase in amplitude of the EMV structures is a key feature of our analysis (see below) that yields important information on the electronic properties of the studied materials.

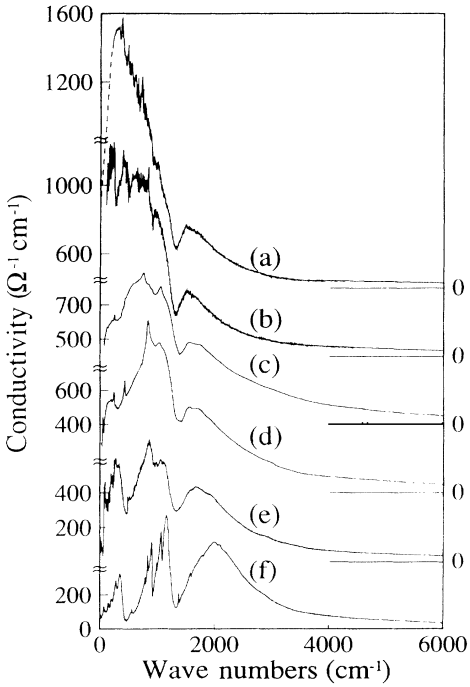

FIG. 2. **E||a** polarized infrared conductivity spectra (15–6000 cm^{-1}) of (a) $(TMTSF)_2ClO_4$; (b) $(TMTSF)_2PF_6$; (c) $(TMTSF)_2BF_4$; (d) $(TMTSF)_2ReO_4$; (e) $(TMTTF)_2Br$; (f) $(TMTTF)_2PF_6$ at room temperature. The spectra (c) and (d) have been obtained by Kramers–Kronig transformation of the reflectivity data of Homes and Eldridge from Refs. 22, 23.

IV. MODEL ANALYSIS

At room temperature all the studied materials are isostructural.[33–38] They crystallize in the triclinic system (space group $P\bar{1}$, $Z = 1$) with the molecular stacks parallel to the crystallographic **a** axis. The molecules are piled in a zigzag arrangement with their molecular planes almost perpendicular to the stacking axis. The columns are arranged side by side to form sheets parallel to the (001) plane separated in the **c** direction by sheets of anions. The two organic molecules in a unit cell lie on general positions and are connected by inversion symmetry points. A schematic side view of the stacks is sketched in Fig. 3 where the horizontal bars represent the planar molecules and the large crosses the counteranions. Within a stack, the interplanar distances d_1 and d_2 show a slight alternation corresponding to a small dimerization. The amplitude of the lattice dimerization, $\Delta d = |d_1 - d_2|$, varies from salt to salt, being greater in the sulfur-containing materials. The counteranions are placed out of the molecular planes along alternate directions so that the TMTSF stacks experience from them a potential of period **a** with its maxima (and minima) centered between the molecular planes.

By stoichiometry (one electron is fully transferred to the inorganic anion), the one-electron structure consists of quarter-filled hole bands. According to currently accepted criteria, the room-temperature electronic structure can be considered as quasi-1D[4,39] and the open Fermi surface is made up of two warped planes at $\mathbf{k}_F = \pm\mathbf{a}^*/4$. The gap due to the dimerization and to the anion potential opens at $\pm\mathbf{a}^*/2$, that is, away from the Fermi surface so that transport and optical properties are little affected by its presence in the one-electron picture. We have estimated that a gap of the expected amplitude implies a transfer of only a few percent of the oscillator strength from intraband to interband optical transitions.[7,17] As a matter of fact, marked deviations from a simple Drude behavior are experimentally observed for most organic molecular conductors, notably quarter-filled dimerized ones.[9,17,28] The most apparent among them are (i) a shift of the conductivity maximum from zero frequency, and the associated appearance of optical gaps or pseudogaps; (ii) the appearance of structures in the spectrum attributable to EMV and electron–intermolecular-phonon (EIP) couplings; (iii) deviations from the partial optical sum rule.[9,21]

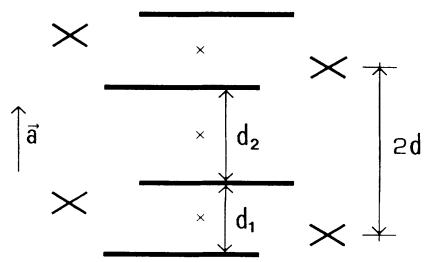

FIG. 3. Schematic side view of a single molecular stack surrounded by the inorganic counteranions. Horizontal bars represent the planar molecules and large crosses the counteranions. d_1 and d_2 are the alternating interplanar distances in the dimerized stack.

Previous work[7,17,18] has shown that it is possible to account for most of the properties of the infrared spectra of dimerized quarter-filled conductors in terms of a model we have previously developed for the optical properties of an infinite molecular chain system with coupling of electrons to intra- and intermolecular phonons and to a static potential.[14] Successful results can however be obtained only by considering an electronic band structure in which doubly occupied states are forbidden. The applicability of this model to a wide series of Bechgaard salts and the implication of the results are the subject of the rest of this paper.

A. Dimerized molecular chain model

The dimerized molecular chain model[14] was originally developed for a 1D molecular chain system carrying general twofold commensurate charge-density waves (CDW's) with components centered between the molecular sites, i.e., on the bonds (b-CDW) and on the molecular sites (s-CDW). Structurally, this corresponds to including a lattice dimerization (LD) and an alternating molecular deformation (AMD). It should be noted that, by virtue of their crystal symmetry, the Bechgaard salts and their sulfur analogs at room temperature can only bear a b-CDW since all molecular sites are equivalent. In the following we shall then briefly outline the model in the corresponding reduced form.

The model system consists of an assembly of noninteracting molecular chains composed of N identical molecules. Each chain is subject to a LD whose amplitude is $\Delta d = 4u_0$ where u_0 is the longitudinal displacement of the molecules from their location in the *undistorted* chain. The LD corresponds to a periodic lattice distortion whose period is twice the regular chain spacing d, hence the wave vector of the LD is $q_0 = \pi/d$. The electrons in the chains are also subjected to a static potential, say from the inorganic anion chains and from some mean-field electron correlation, of period $2d$ acting between sites, i.e., on the bonds, with an amplitude B_x. The electrons are also coupled to an arbitrary number of intramolecular vibrational modes and to one longitudinal acoustic phonon branch.

In the site representation the corresponding Hamiltonian for a single chain is

$$H = H_E + H_{EV} + H_V \ , \tag{2}$$

with

$$H_E = -t\sum_{n,\sigma}(a^\dagger_{n+1,\sigma}a_{n,\sigma} + \text{H.c.}) + \frac{\Delta_b}{2}\sum_{n,\sigma}(-1)^n(a^\dagger_{n+1,\sigma}a_{n,\sigma} + \text{H.c.}) \ , \tag{3}$$

where $a_{n,\sigma}$ ($a^\dagger_{n,\sigma}$) is the annihilation (creation) operator for an electron or hole of spin $\sigma = \pm 1/2$ on the nth site, t is the transfer integral for the regular chain, and

$$\Delta_b = 2B_x + \left(\frac{\partial t}{\partial u}\right)_0 4u_0 \ . \tag{4}$$

$\Delta_b/2$ represents an alternating modulation of the average transfer integral t produced by the static potential and the chain dimerization. The latter contribution represents the static effect of the coupling of the electronic system to the longitudinal acoustic phonon at q_0. Such a coupling is expressed by the derivative $(\partial t/\partial u)_0$ calculated at the equilibrium position of the molecules in the undistorted chain.

The dynamic coupling of the electrons to v intramolecular vibrational modes and to one intermolecular phonon mode is expressed in the usual way by

$$H_{EV} = \sum_{i=1}^{v}\sum_{n,\sigma} g_i q_{n,i} a^{\dagger}_{n,\sigma} a_{n,\sigma} - \sum_{n,\sigma}\left(\frac{\partial t}{\partial u}\right)_0 (u_{n+1}-u_n)(a^{\dagger}_{n+1,\sigma}a_{n,\sigma} + \text{H.c.}) \ . \tag{5}$$

As customary,[40,41] the linear EMV coupling constant is $g_i = (\partial\epsilon/\partial q_i)_0$ where ϵ is the unpaired-electron molecular orbital energy and q_i is the ith dimensionless intramolecular normal coordinate, which is bound by symmetry to be totally symmetric in order to give a nonzero linear coupling constant with a nondegenerate molecular orbital.[40–42] The derivative is calculated at the equilibrium geometry of the molecule carrying a formal fractional charge of ρ electrons or holes. The EIP coupling is expressed linearly through the modulation of the transfer integral t by the longitudinal displacement u_n of the molecules from their equilibrium location in the *distorted* chain.[41,43] H_V is the vibrational Hamiltonian in the harmonic approximation.

The representation of the one-electron Hamiltonian H_E in the reciprocal space (with k ranging over the extended Brillouin zone from $-\pi/d$ to π/d) is

$$H'_E = \sum_{k,\sigma}\epsilon_k a^{\dagger}_{k,\sigma}a_{k,\sigma} + \sum_{k,\sigma}\Delta_k a^{\dagger}_{k+q_0,\sigma}a_{k,\sigma} \ , \tag{6}$$

where

$$\epsilon_k = -2t\cos(kd) \ , \tag{7}$$

and

$$\Delta_k = i\Delta_b \sin(kd) \ . \tag{8}$$

Equation (6) is the Hamiltonian of a split tight-binding band and can be reduced to a diagonal form, $H'_E = \sum_{kn,\sigma} E_{kn} A^{\dagger}_{kn,\sigma} A_{kn,\sigma}$, by the transformation

$$a_{k+lq_0,\sigma} = \sum_n f_{nl}(k) A_{kn,\sigma} \qquad (n,l=0,1) \ , \tag{9}$$

where

$$f_{n0}(k) = \frac{-(\epsilon_k + E_{kn})}{[(\epsilon_k+E_{kn})^2 + |\Delta_k|^2]^{1/2}} \ , \qquad f_{n1}(k) = \frac{-\Delta_k}{[(\epsilon_k+E_{kn})^2 + |\Delta_k|^2]^{1/2}} \ , \tag{10}$$

and

$$E_{kn} = (-1)^{n+1}(\epsilon_k^2 + |\Delta_k|^2)^{1/2} \qquad (n=0,1) \ . \tag{11}$$

E_{kn} are the energies of two tight-binding bands separated by a gap of amplitude $2|\Delta_b|$ located at the boundaries $(-\pi/2d, \pi/2d)$ of the reduced zone of the distorted chain. From Eq. (4) the gap structure depends on the amplitude of the static potential B_x, the coupling constant $(\partial t/\partial u)_0$, and the amplitude of the chain dimerization u_0. In addition, the last two parameters are related to the gap amplitude Δ_b by the self-consistent relation

$$u_0 = \frac{4\Delta_b}{NM\omega_e^2(q_0)}\left(\frac{\partial t}{\partial u}\right)_0 \times \sum_k \frac{\sin^2(kd)[n(E_{k0}) - n(E_{k1})]}{(\epsilon_k^2 + |\Delta_k|^2)^{1/2}} \ , \tag{12}$$

where M is the molecular mass, $\omega_e(q_0)$ is the unrenormalized frequency of the acoustic mode at the Brillouin zone boundary, and $n(\epsilon)$ is the appropriate distribution function (see below). If any two of the parameters u_0, $(\partial t/\partial u)_0$, B_x and Δ_b are known, say from structural and spectroscopic data, the other two are uniquely determined by the use of Eqs. (4) and (12) . This allows us to estimate the individual contributions of the acoustic phonon and the static potential to the total gap.

By Fourier transforming Eq. (5) and applying the transformation Eq. (9), the coupling term H_{EV} reads:

$$H'_{EV} = \sum_{k,q,\sigma}\sum_{\nu,n,m}\left[V^e_{\nu nm}(k,q)Q_e(q+\nu q_0) + \sum_{i=1}^{v} V^i_{\nu nm}(k,q)Q_i(q+\nu q_0)\right] A^{\dagger}_{k+q,n,\sigma}A_{k,m,\sigma} \ , \tag{13}$$

where $\nu = 0, 1$, $Q_e(q)$, and $Q_i(q)$ are the Fourier components (in the extended zone representation) of the inter- and intramolecular coupled modes, respectively, and:

$$V^e_{\nu nm}(k,q) = \frac{1}{\sqrt{N}}\sum_{l=0}^{1} g_e(k+lq_0, q+\nu q_0) \times f^*_{n,l+\nu}(k+q) f_{ml}(k) \ , \tag{14}$$

$$V^i_{\nu nm}(k,q) = \frac{1}{\sqrt{N}}\sum_{l=0}^{1} g_i f^*_{n,l+\nu}(k+q) f_{ml}(k) \ , \tag{15}$$

are the coupling constants in the reciprocal space. The usual coupling constant for acoustic phonons[43] $g_e(k,q) = 2i(\partial t/\partial u)_0\{\sin(kd) - \sin[(k+q)d]\}$ has been introduced in Eq. (14).

The infrared optical properties of the model are defined through the complex dielectric function

$$\hat{\varepsilon}(\omega) = \varepsilon_\infty + \hat{\varepsilon}_{\text{inter}}(\omega) + \hat{\varepsilon}_{\text{intra}}(\omega) \ . \tag{16}$$

In Eq. (16) ε_∞ is the core dielectric constant which is usually taken as real. $\hat{\varepsilon}_{\text{inter}}(\omega)$ is the interband contribution deriving from the direct electronic transitions from the lower band $|k,0\rangle$ to the upper one $|k,1\rangle$, and from the vibronic coupling of these transitions with the

inter- and intramolecular vibrational modes. $\hat{\varepsilon}_{\text{intra}}(\omega)$ is the intraband contribution deriving from the electronic transitions within a single energy band. Corresponding to the random-phase approximation, for the calculation of the matrix elements of H'_{EV} in Eq. (13) we replace the phonon coordinate operators by their average value, $\langle Q_\alpha(q,\omega)\rangle$ $(\alpha = e,i;\ i = 1,\ldots,v)$, oscillating at the same frequency as the applied field $\mathcal{E}(\omega)$.

Calculation of the interband contribution to the dielectric function in the linear response approximation yields

$$\hat{\varepsilon}_{\text{inter}}(\omega) = -\frac{4\pi}{NV_m}\left[\chi(\omega) + \sum_\alpha \chi_\alpha(\omega)\right] , \tag{17}$$

where V_m is the volume per molecule and $\alpha = e,i$ with $i = 1,\ldots,v$. In the Eq. (17) the first term is the dielectric susceptibility for the single-particle excitation across the gap,

$$\chi(\omega) = \sum_k \sum_{n,m} \frac{\hbar^2}{(E_{kn} - E_{km})^2} \times \frac{n(E_{kn}) - n(E_{km})}{E_{kn} - E_{km} - \hbar\omega - i\hbar\Gamma_{\text{inter}}} |j_{nm}(k)|^2 , \tag{18}$$

where Γ_{inter} is a phenomenological damping parameter for the electronic interband transitions, and $j_{nm}(k) = \langle kn,\sigma|j|km,\sigma\rangle$ is a matrix element of the current density operator

$$j = \sum_k \sum_{n,m} [j_s \sin(kd)(f^*_{n0}f_{m0} - f^*_{n1}f_{m1}) + ij_c \cos(kd)(f^*_{n1}f_{m0} - f^*_{n0}f_{m1})] A^\dagger_{kn,\sigma}A_{km,\sigma} , \tag{19}$$

with

$$j_s = -\frac{2e}{\hbar}(td + u_0\Delta_b) , \tag{20}$$

$$j_c = -\frac{2e}{\hbar}\left(2tu_0 + d\frac{\Delta_b}{2}\right) . \tag{21}$$

The terms in the summation of Eq. (17)

$$\chi_\alpha(\omega) = \frac{\langle Q_\alpha(\omega)\rangle}{\mathcal{E}(\omega)} \sum_k \sum_{m,n} \frac{i\hbar}{E_{kn} - E_{km}} \times \frac{n(E_{kn}) - n(E_{km})}{E_{kn} - E_{km} - \hbar\omega - i\hbar\Gamma_{\text{inter}}} \times V^\alpha_{1mn}(k,0) j_{nm}(k) , \tag{22}$$

account for the spectroscopic effects deriving from the vibronic couplings of the electrons with the intra- and intermolecular phonons. The average values of the phonon coordinates $\langle Q_\alpha(q,\omega)\rangle$ are calculated by solving the set of $(v+1)$ linear coupled equations defined in Eqs. (3.7)–(3.10) of Ref. 14. For systems carrying only a b-CDW, like those considered, the vibronic susceptibilities $\chi_\alpha(\omega)$ are nonzero only for the intramolecular modes $(\alpha = i)$ that derive their vibronic activity from the phase oscillations of the b-CDW.

For the intraband contribution to the dielectric function, the model assumes a Drude-like behavior[21]

$$\hat{\varepsilon}_{\text{intra}}(\omega) = -\omega_p^2/(\omega^2 + i\omega\Gamma_{\text{intra}}) , \tag{23}$$

where ω_p and Γ_{intra} are the plasma frequency and a phenomenological damping parameter for the electronic intraband transitions, respectively. The plasma frequency is calculated from the band structure in the self-consistent-field approximation[21]

$$\omega_p^2 = \frac{4\pi e^2}{\hbar^2 NV_m} \sum_{k,n} n(E_{kn}) \frac{\partial^2 E_{kn}}{\partial k^2} . \tag{24}$$

When the dimerized chain model is used to calculate the optical properties of a system containing an average number of carriers per molecule $\rho = 0.5$, that is, a quarter-filled band system (with reference to the undistorted structure), it yields markedly different results depending on the form adopted for the distribution function $n(\epsilon,T)$. In particular, we have considered

$$n_\xi(\epsilon,T) = \xi\left[1 + \frac{\xi}{2}\exp\left(\frac{\epsilon - E_F^{(\xi)}(T)}{k_BT}\right)\right]^{-1} . \tag{25}$$

If one assumes $\xi = 2$, Eq. (25) is simply the Fermi-Dirac distribution function with an additional factor of 2 to embody the summation over the spin degrees of freedom. It is therefore appropriate when the carriers are assumed to behave as ordinary electrons or holes. With $\xi = 1$, Eq. (25) describes the statistics for carriers behaving as spinless fermions. It is appropriate when the double occupancy of the band states is forbidden. In the simple Hubbard model this occurs when the U/t ratio tends to infinity.[20] The two different statistics of course imply two different locations for the Fermi energy and wave vector. At $T = 0$ K, with $\xi = 2$ the lower band is half filled and the Fermi wave vector is at $\pi/4d$ whereas with $\xi = 1$ the Fermi energy is at the center of the dimerization gap[44] and the Fermi wave vector is at the Brillouin zone limit. At finite temperatures, $[E_F(T)]_{\xi=1} = -k_BT\ln 2$.[44]

The optical properties calculated using the dimerized chain model with $\xi = 1$ or with $\xi = 2$ display remarkable differences which are conveniently discussed with reference to the infrared conductivity spectrum. As the dimerization opens a gap away from the Fermi surface in the $\xi = 2$ case, at dimerization amplitudes on the order of those commonly found in quarter–filled molecular conductors ($\lesssim 10\%$ of the total bandwidth), the transfer of oscillator strength from intraband to interband transitions is only a few percent.[17,7] Thus, the infrared conductivity remains essentially Drude-like with a maximum at zero frequency and a small bump due to interband transitions at energies of order $\hbar\omega = 4t$.

The $\xi = 1$ case produces a conductivity spectrum which is dominated by interband transitions with an onset at the dimerization gap energy $\hbar\omega = 2\Delta_b$. Thus, at low temperatures the conductivity maximum clearly shifts at finite frequency (Fig. 4, full curve). At high temperatures when the dimerization gap is of order k_BT, a Drude-like intraband contribution coming from the thermally excited carriers may partially mask the optical gap (Fig. 4, dashed curve). However, even for small dimerization gaps the most distinctive feature of the optical spectra calculated for the $\xi = 1$ case is the presence of

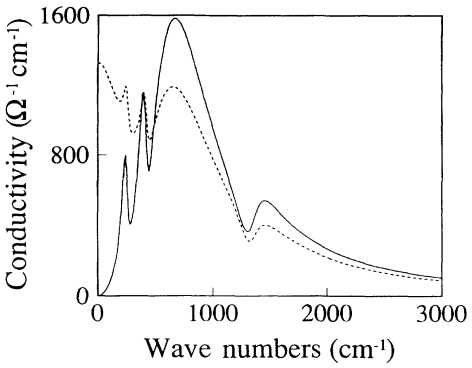

FIG. 4. Conductivity spectra calculated according to the dimerized molecular chain model in the $\xi = 1$ scheme. Full curve: $T = 0$ K spectrum consisting of interband transitions only; dashed curve: room-temperature spectrum including intraband transitions.

well-defined vibronic structures in the midinfrared frequency region. This is due to the fact that in the dimerized chain model the vibronic structures derive from the EMV coupling involving the interband transitions only [cf. Eq. (17)]. In the $\xi = 2$ case, such transitions occur at markedly higher energy and with much smaller oscillator strength than in the $\xi = 1$ case. Thus the vibronic features are vanishingly small and practically undetectable unless the dimerization gap becomes comparable to the bandwidth.

At higher order of perturbation theory the optical spectra may display features attributed to the coupling with intraband transitions. This is known as the Holstein effect[45,46] and is expected to yield spectroscopic features weaker and of a different shape with respect to those considered in our model. In ordinary metals and superconductors the Holstein effect is observed only at low temperatures.[47] In the discussion to follow we make the reasonable assumption that the contribution of the Holstein effect to our room-temperature spectra can be neglected.[48]

The previously reported results[15–17] obtained by comparing experimental data with calculations carried out for the $\xi = 2$ and $\xi = 1$ cases have shown that only the latter is capable of reproducing satisfactorily the measured spectra. The fact that distinctive vibronic structures can be observed in all the spectra of Fig. 2 has prompted us to use the same scheme in the analysis of the experimental data presented in the following section.

B. Fitting of the experimental data

Our analysis of the room-temperature infrared data of the studied materials has been based on the comparison of the experimental stack-axis-polarized reflectance and conductivity spectra with those calculated through the 1D model mentioned above in the spinless-fermion, $\xi = 1$, case. As noted in Sec. III the most important features of the conductivity data shown in Fig. 2 are the location of the main conductivity peak at finite frequencies, i.e., the existence of an optical gap, and the presence of vibronic structures whose intensities are strongly correlated with the amplitude of the gap. In particular, as the principal maximum of the conductivity shifts to higher frequencies the vibronic structures become increasingly pronounced. This behavior appears to be correlated with the amplitude of the stack dimerization and becomes particularly evident in going from TMTSF to TMTTF compounds when the dimerization amplitude becomes greater. A key point of our analysis has been to investigate quantitatively the existing correlations between dimerization amplitude, optical gap, and location and intensity of the vibronic structures by comparing measured and calculated spectra for the series of compounds $(TMTSF)_2ClO_4$, $(TMTSF)_2PF_6$, $(TMTSF)_2BF_4$, $(TMTSF)_2ReO_4$, $(TMTTF)_2Br$, and $(TMTTF)_2PF_6$, which display an increasing stack dimerization and a correlated increasing amplitude of the optical gap.

For the calculation, in the $\xi = 1$ scheme, of the room-temperature stack-polarized optical functions $R(\omega)$ and $\sigma(\omega)$, the input parameters include (i) the structural parameters, namely the average interplanar distance between the molecules within the stack $d = |\mathbf{a}|/2 = |d_1 + d_2|/2$, the amplitude of the LD, $u_0 = \Delta d/4$, and the molecular volume V_m; (ii) the electronic parameters, that is the average charge transfer integral t, the gap amplitude Δ_b, the damping factors for the intra- and interband electronic transitions Γ_{intra} and Γ_{inter}, and the dielectric core constant ε_∞; (iii) the molecular mass M, the frequency ω_e, and the damping factor γ_e, of the coupled intermolecular phonon; (iv) the frequencies ω_i, the EMV coupling constants g_i, and the damping factors γ_i of the v coupled intramolecular totally symmetric modes.

A limited number of input parameters have been adjusted to fit the experimental data. The values of the structural parameters have been derived from the room-temperature structural data, which are known for all the studied compounds.[33–38] Also the frequencies of the totally symmetric vibrational modes of the neutral TMTTF and TMTSF molecules and of their radical cations are well known.[24] In particular, for the frequencies ω_i of the coupled intramolecular modes we have adopted values appropriate for the isolated TMTTF or TMTSF molecules with a formal charge of $\rho = 0.5$. These values have been estimated by taking the average of the frequencies of the neutral molecule and of the corresponding radical cation. Owing to the poor knowledge of the intermolecular modes in the studied compounds, we have used an effective fixed value for the frequency of the single coupled acoustic phonon. On the basis of the available literature data,[49,50] values of 50 cm^{-1} and 10 cm^{-1} have been assigned to the parameters ω_e and γ_e, respectively. Therefore the only adjustable parameters are the average transfer integral t, the gap amplitude Δ_b, the EMV constants g_i, the damping factors Γ_{inter}, Γ_{intra}, and γ_i, and the dielectric core constant ε_∞. The EIP coupling constant $(\partial t/\partial u)_0$ and the amplitude of the anionic potential B_x have been estimated in a self-consistent way using the relations (4) and (12) of Sec. IV A. This has permitted us to disentangle the phononic and anionic contributions to the gap amplitude.

The general criterion adopted to analyze the exper-

imental data has been to reproduce simultaneously all the principal spectral features of both the conductivity and reflectance spectra. It is noteworthy that each of these spectral features is affected mainly by one definite model parameter. This has allowed us to identify rather unique and reliable sets of parameters even though the goodness of the fit could only be appreciated by visual inspection. Attempts at performing least-squares fittings by the use of the available computer routines for data analysis proved to be impractical because of the lengthy calculations required.

The experimental and calculated reflectance spectra in the range 15–9000 cm^{-1} and the corresponding experimental and calculated conductivity spectra in the range 15–3000 cm^{-1} are reported in Fig. 5 and Fig. 6, respectively, for the six studied compounds $(TMTSF)_2ClO_4$, $(TMTSF)_2PF_6$, $(TMTSF)_2BF_4$, $(TMTSF)_2ReO_4$, $(TMTTF)_2Br$, and $(TMTTF)_2PF_6$. For the two compounds $(TMTSF)_2BF_4$ and $(TMTSF)_2ReO_4$, the experimental reflectance data are those recently reported by Homes and Eldridge.[22,23] As shown in the figures, the $\xi = 1$ calculations allow a satisfactory fit of both the conductivity and reflectance spectra for all the studied materials. Note that the integrated areas, the reflectance values and the location of the plasma edges, the conductivity levels in the infrared, and the EMV structures are simultaneously fitted to a quite satisfactory level of accuracy. In going from $(TMTSF)_2ClO_4$ to $(TMTTF)_2PF_6$ through the series of studied compounds, the experimental reflectance and conductivity spectra show increasing deviations from simple Drude behavior, correlated with the decrease of the dc conductivity and the increase of the stack dimerization. The level of the midinfrared reflectance decreases and the dispersive vibronic structures become more apparent. In the conductivity spectra such deviations are perhaps more evident. They display an increasing optical gap and a corresponding enhancement of the vibronic structures whose band shapes also depend on the gap amplitude. The overview provided by Figs. 5 and 6 allows one to conclude that the spinless-fermion calculations are indeed able to reproduce in a quite accurate manner the progressive changes of shape of the experimental reflectance and conductivity spectra for the full sequence of the studied materials.

The values of the electronic parameters used for the calculations are reported in Table I along with the relevant structural parameters, d, Δd, and V_m taken from the literature. The values of the average transfer integral t range from 0.27 eV for $(TMTSF)_2ClO_4$ and $(TMTSF)_2BF_4$ to 0.18 eV for $(TMTTF)_2PF_6$, which correspond to full bandwidths ($W = 4t$) of 1.08 and 0.72 eV, respectively. The gap amplitude $2\Delta_b$ increases from 0.050 to 0.174 eV in going from $(TMTSF)_2ClO_4$ to $(TMTTF)_2PF_6$. These are, respectively, the most *metallic* and the most dimerized of the six studied compounds. For the TMTSF salts the gap amplitude is small and represents about 5%–9% of the total bandwidths. For the TMTTF salts the percentage gap amplitude is larger, ranging from 12% up to 24%.

In our model calculations the gap opens at the Fermi surface, which is shifted to the reduced zone bound-

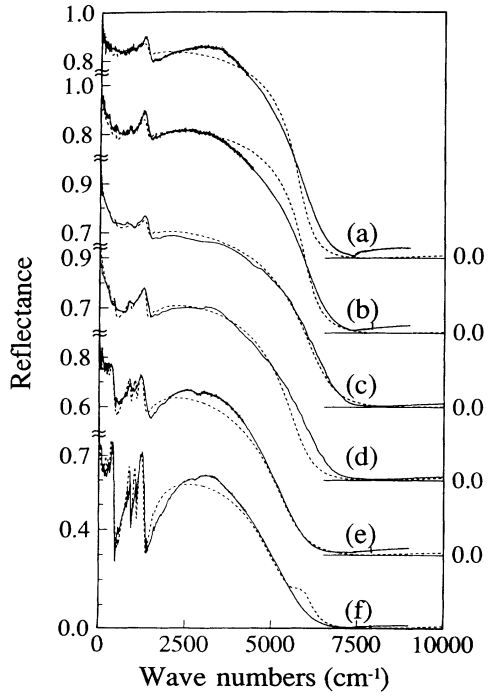

FIG. 5. Room-temperature experimental (full curves) and calculated (dashed curves) **E**||**a** reflectance spectra of (a) $(TMTSF)_2ClO_4$; (b) $(TMTSF)_2PF_6$; (c) $(TMTSF)_2BF_4$; (d) $(TMTSF)_2ReO_4$; (e) $(TMTTF)_2Br$; (f) $(TMTTF)_2PF_6$ in the range 15–9000 cm^{-1}.

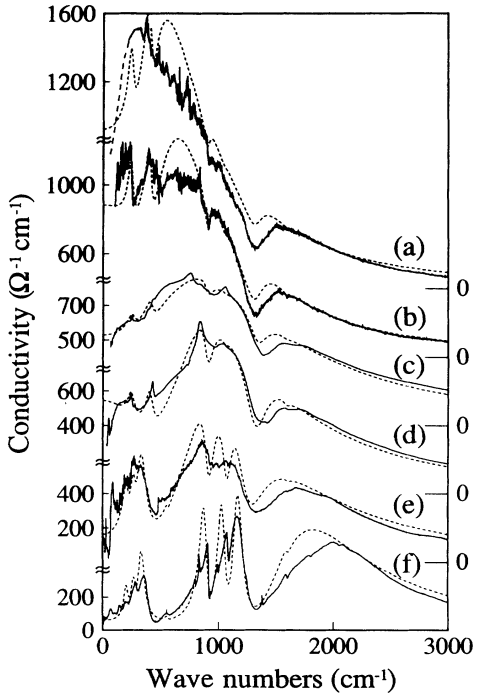

FIG. 6. Room-temperature experimental (full curves) and calculated (dashed curves) **E**||**a** conductivity spectra of (a) $(TMTSF)_2ClO_4$; (b) $(TMTSF)_2PF_6$; (c) $(TMTSF)_2BF_4$; (d) $(TMTSF)_2ReO_4$; (e) $(TMTTF)_2Br$; (f) $(TMTTF)_2PF_6$ in the range 15–3000 cm^{-1}.

TABLE I. Structural and electronic interaction parameters for $(TMTSF)_2X$ and $(TMTTF)_2X$ salts.

	$(TMTSF)_2X$				$(TMTTF)_2X$	
	ClO_4^- [a]	PF_6^- [b]	BF_4^- [c]	ReO_4^- [d]	Br^- [e]	PF_6^- [f]
d (Å)	3.63	3.64	3.62	3.64	3.51	3.57
Δd (Å)	0.01	0.03	0.03	0.00	0.03	0.10
V_m (Å^3)	347.2	357.2	342.2	355.2	308.2	337.8
t (eV)	0.27	0.25	0.27	0.25	0.20	0.18
Δ_b (eV)	0.025	0.031	0.032	0.046	0.050	0.087
Γ_{inter} (cm^{-1})	250	300	650	450	500	300
Γ_{intra} (cm^{-1})	600	450	800	400	1000	500
ε_∞	2.30	2.00	2.00	2.20	2.10	2.00

[a]Structural data from Ref. 33.
[b]Structural data from Ref. 34.
[c]Structural data from Ref. 35.
[d]Structural data from Refs. 36–38.
[e]Structural data from Refs. 37 and 38.

aries for spinless fermions. This qualifies all the studied compounds as narrow-gap 1D semiconductors. For the TMTSF materials, and also for $(TMTTF)_2Br$, the gap amplitude amounts to just a few (2–4) k_BT at room temperature and the experimentally observed dc conductivities are easily accounted for in terms of the contribution from thermally excited carriers. The intraband optical transitions involving these carriers are responsible for the finite far-infrared conductivity observed for the TMTSF compounds. Note that the plasma frequency, that is, the intraband oscillator strength, is calculated through Eq. (24) using the same values of t and Δ_b as for the rest of the spectrum. The only adjustable parameter with regard to the intraband transitions is Γ_{intra}.

We wish to emphasize that the picture of these materials as correlated semiconductors stems from our analysis of the room-temperature optical data and it is not meant to apply to other temperature or pressure regimes. As discussed in more detail in the following section, whereas most of the TMTTF salts behave as 1D semiconductors also at lower temperatures, there is experimental evidence of a metalliclike behavior of the crystals with smaller dimerization gap, namely the $(TMTSF)_2X$ salts, among which are those that become superconductors.

Inasmuch as our calculations succeed in reproducing the vibronic effects in the reflectance and conductivity spectra, the analysis of the measured data yields additional important information concerning the EMV and EIP coupling. Tables II and III report the values of the frequencies ω_i, the EMV coupling constants g_i, and the damping factors γ_i, of the coupled intramolecular modes used to fit the experimental data of TMTSF and TMTTF compounds, respectively. It should be noted that the same set of EMV coupling constants has been used for the four TMTSF salts and, with some expected modifications, also for the two TMTTF salts. This clearly reflects the fact that, to a fairly good level of approximation, the EMV coupling constants are molecular properties that carry over from one crystal to another.

V. DISCUSSION

Table IV reports the parameters of the electronic structure of the studied compounds as deduced from our analysis of the optical spectra. Beside determining the contribution of the interband transitions, the same parameters, through Eq. (24), account for the oscillator strength of the intraband transitions expressed by the plasma frequency ω_p. Also reported are the optical relaxation time $\tau = 1/(2\pi c\Gamma_{intra})$ and the zero-frequency optical conductivity of the Drude model $\sigma_{opt}(0) = \omega_p^2\tau$. For the sake of comparison with the values of the fitting parameters, Table IV also reports the average values of the intrastack transfer integrals calculated by quantum-chemical methods using different orbital basis sets,[52–54] and two sets of values for the room-temperature dc con-

TABLE II. Frequencies, coupling constants, and damping factors of the coupled totally symmetric intramolecular modes of TMTSF.

a_g mode no.[a]	ω_i (cm^{-1})[a]	g_i (eV)	γ_i (cm^{-1})[b]	γ_i (cm^{-1})[c]
ν_3	1599	0.04	20	30
ν_4	1469	0.10	20	30
ν_7	1060	0.01	20	30
ν_8	920	0.03	20	30
ν_9	452	0.04	20	30
ν_{10}	282[d]	0.03	20	30

[a]From Ref. 24.
[b]From Ref. 51.
[c]For $(TMTSF)_2PF_6$ and $(TMTSF)_2ClO_4$.
[d] For $(TMTSF)_2BF_4$ and $(TMTSF)_2ReO_4$.

TABLE III. Frequencies, coupling constants, and damping factors of coupled totally symmetric intramolecular modes of TMTTF.

a_g mode no.[a]	ω_i (cm^{-1})[a]	g_i (eV)	γ_i (cm^{-1})
ν_3	1603	0.03	20
ν_4	1478	0.12	30
ν_7	1098	0.03	20
ν_8	938	0.03	20
ν_9	563	0.02	10
ν_{10}	508	0.06	30
ν_{11}	288	0.01	20
ν_{12}	222	0.01	20

[a]From Ref. 24.

ductivity. The first one, σ_{dc}, comes from direct experimental measurements,[55–58] whereas the second one, σ_{HR}, reports the values assumed by the dc conductivity in our Hagen–Reubens extrapolations of the experimental reflectance data see [Eq. (1)].

In going from $(TMTSF)_2ClO_4$ to $(TMTTF)_2PF_6$, the parameters of the electronic structure follow coherently the changes of the crystal structures and of the transport properties. In particular, the values of the estimated average transfer integral t scale properly with those of the calculated ones, reported in Table IV, and with the average interplanar spacing d shown in Table I. In terms of absolute magnitudes, the t values estimated from optical data are much closer to those calculated using single-ζ (Refs. [52,53]) rather than double-ζ (Ref. 54) atomic orbitals, despite the fact that the latter basis set is assumed to yield more accurate results. Drude analyses of the plasma edge in room-temperature reflectance spectra of $(TMTSF)_2ClO_4$,[26] $(TMTSF)_2PF_6$,[28] and $(TMTTF)_2PF_6$,[28] have given values of the transfer integrals of 0.23, 0.25, and 0.20 eV, respectively. These values are rather close to our estimates although our analysis is based on a quite different model.

The width of the gap Δ_b displays the right tendency to increase as the dimerization amplitude Δd increases and the dc conductivity decreases as shown in Tables I and IV. Note that the features of the spectra depend on the gap amplitude Δ_b but are insensitive to the specific driving force for the formation of the b-CDW which originates the gap. Useful information on the mechanism for the b-CDW formation can be gained by the use of the self-consistent relations Eqs. (4) and (12), along with the available structural information. For all the studied materials, independent of the inorganic counteranion, the contribution of the static potential $2B_x$ accounts for almost all of the dimerization gap Δ_b. That means that the gap is brought about mainly by the effect of a $4k_F$ static potential rather than from a phonon-induced Peierls mechanism. This is *a priori* evident for the case of $(TMTSF)_2ReO_4$ whose reported crystal structure exhibits a vanishing dimerization amplitude. Note that this would also imply a vanishing EIP coupling constant. By using for the constant $(\partial t/\partial u)_0$ the largest value found for the other compounds, that is, 0.15 eV $Å^{-1}$, the anionic contribution is still prevalent (86% of the total gap amplitude) and the corresponding self-consistent value for the stack dimerization amplitude is 0.04 Å, a value in the same range as those found for the other $(TMTSF)_2X$ compounds.

The values found for the effective EIP coupling constant $(\partial t/\partial u)_0$ are affected by some uncertainty. We do not base our estimates of $(\partial t/\partial u)_0$ on direct experimental data. In fact for a dimerized stack displaying only a b-CDW, the totally symmetric intermolecular modes responsible for the modulation of the intrastack transfer integral are not infrared active.[14] Our estimates, based on self-consistency criteria, consider only one effective coupled mode modulating the intermolecular distances along the stack. Owing to the dependence on the square of the intermolecular mode frequency ω_e [see Eq. (12)], our $(\partial t/\partial u)_0$ estimates are strongly dependent on the value assumed for this frequency. The $(\partial t/\partial u)_0$ values

TABLE IV. Transfer integrals, gap properties, EIP coupling constant, plasma frequency, and transport properties for $(TMTSF)_2X$ and $(TMTTF)_2X$ salts. (See text for the definition of symbols.)

	$(TMTSF)_2X$				$(TMTTF)_2X$	
	ClO_4^-	PF_6^-	BF_4^-	ReO_4^-	Br^-	PF_6^-
t (eV)	0.27	0.25	0.27	0.25	0.20	0.18
t_{calc} (eV)[a]	0.24	0.23		0.23	0.13	0.11
t_{calc} (eV)[b]	0.37	0.36		0.36	0.24	
Δ_b (eV)	0.025	0.031	0.032	0.046	0.050	0.087
$2B_x$ (%)	97.	86	86	100	97	88
$(\partial t/\partial u)_0$ (eV $Å^{-1}$)	0.06	0.15	0.15	0.00	0.05	0.11
ω_p (cm^{-1})	5763	4881	5038	3614	3135	1323
τ (10^{-15} s)	8.85	11.80	6.64	13.27	5.31	10.62
$\sigma_{opt}(0)$ (Ω^{-1} cm^{-1})	922	882	529	544	163	58
σ_{dc} (Ω^{-1} cm^{-1})	670[c]	540[d]	540[d]	300[e]	240[f]	40[f]
σ_{HR} (Ω^{-1} cm^{-1})	690	500	540	300	160	40

[a]From Refs. 52 and 53.
[b]From Ref. 54.
[c]From Ref. 55.
[d]From Ref. 56.
[e]From Ref. 57.
[f]From Ref. 58.

reported in Table IV have been obtained assuming for ω_e the reasonable value of 50 cm^{-1}.[49,50] With a presumably overestimated value of 100 cm^{-1} for ω_e we obtain for $(\partial t/\partial u)_0$ values in the range 0.20–0.60 eV $Å^{-1}$, with a corresponding $2B_x$ contribution to the gap of 88% and 42% respectively.

The knowledge concerning the EIP coupling is quite poor. This is principally due to the fact that both the frequencies and the coupling constants of the intermolecular modes are strongly dependent on the crystal structures. This prevents the transferability of the experimental data from one structure to another, and makes it difficult to compare our estimated $(\partial t/\partial u)_0$ values with those of previous works. For $(TMTSF)_2PF_6$ there are some theoretical and experimental indications. Semiempirical quantum-chemical calculations,[59] based on a single-ζ basis set, indicate values in the range 0.20–0.35 eV $Å^{-1}$. One phonon scattering analysis of the low-temperature resistivity data[60] gives a value of about 0.31 eV $Å^{-1}$; this estimate is however dependent on the frequency of the scattered intermolecular phonon and on the total bandwidth. Using our value for the $(TMTSF)_2PF_6$ bandwidth, the EIP coupling constant value rises to 0.45 eV $Å^{-1}$. The above discussion demonstrates that the present indirect estimates and calculations of the EIP coupling constants are still affected by a rather large degree of uncertainty.

For the $\xi = 1$ calculations, when the gap amplitudes are of the order k_BT, as is the case of the studied compounds at room temperature, there is a strong Drude-like intraband contribution to the optical functions coming from thermally excited carriers. As illustrated in Fig. 4, this contribution is quite important in determining the shape of the calculated room-temperature conductivity spectra in the low-frequency region. According to Eq. (24), the oscillator strength of the intraband transitions, as expressed by the plasma frequency ω_p, is uniquely fixed by the electronic parameters t and Δ_b. The values of these parameters are, to a very large extent, determined by the other features of the spectra such as the interband transitions, the frequency location of the conductivity maximum, and the vibronic structures. Therefore, in order to reproduce the partial filling of the optical gap presented by the conductivity data, the only free parameter is the optical relaxation time $\tau = 1/(2\pi c\Gamma_{\text{intra}})$. The value chosen for this parameter should also yield a zero-frequency optical conductivity $\sigma_{\text{opt}}(0) = \omega_p^2\tau$ comparable with the directly measured dc conductivity σ_{dc}, as well as with the values (σ_{HR}) assumed by the dc conductivity in our Hagen-Reubens extrapolations of the experimental reflectance data. The values of ω_p reported in Table IV become smaller in going from the most *metallic*—$(TMTSF)_2ClO_4$—to the most *nonmetallic*—$(TMTTF)_2PF_4$—compound, mainly as a consequence of the increasing dimerization gap. As shown in Table IV, the values of $\sigma_{\text{opt}}(0)$ scale as those directly estimated for σ_{dc} and those of σ_{HR}. The values assumed for the relaxation time τ are in an acceptable range[26,28] but do not show any particular trend.

A very important aspect of our fit has been the ability to reproduce the vibronic structures shown by the optical spectra. Particular attention has been devoted to fit the conductivity data, which, by their absorptive character, are more influenced than the reflectance data by the optical gap and by the related vibronic coupling effects. There are two important points to note concerning the two sets of EMV coupling constants g_i for the TMTSF and TMTTF molecules reported in Tables II and III.

First, in our calculations the molecular vibrational frequencies ω_i have not been considered as adjustable parameters but have been fixed to the values appropriate for the *half-ionized* isolated molecules. In this way all the EMV coupling effects, that is, the intensities of the vibronic structures and their frequency shifts in respect to the unperturbed frequencies of the *half-ionized* molecules, are parametrized by the dimerization gap Δ_b and by the EMV coupling constants g_i.

The second point comes from the fact that, by their definition, the EMV coupling constants have to be considered as microscopic molecular properties that are transferable from crystal to crystal. For this reason we have forced the values of the g_i's to be the same for the four $(TMTSF)_2X$ compounds and, with some modifications, also for the two $(TMTTF)_2X$ compounds. In this way we are rather confident in our estimated g_i values for the TMTSF and TMTTF molecules.

The comparison with previous estimates[22,28] is not very informative inasmuch as previous analyses have used different models and consider the unperturbed frequencies ω_i as adjustable parameters. There is perhaps another point to note concerning the expected similarity between the microscopic properties of related molecules like TTF and its derivatives. In fact the TTF, TMTTF, and BEDT-TTF molecules have similar highest occupied molecular orbitals[61,62] with a charge density distribution concentrated near the central region of the molecules, and similar C=C and C–S stretching a_g modes with almost the same values of the vibrational frequencies.[24,61,63–65] With regard to the vibrational modes that involve mostly the central atoms, our estimated values for the EMV coupling constants of the TMTTF molecule are in good agreement with the related ones of TTF obtained by the fitting of experimental data,[66] and those of BEDT-TTF coming from electronic calculations.[64]

The overall strength of the EMV interactions can be measured in terms of the total dimensionless coupling constant $\lambda = \sum_{i=1}^{v}\lambda_i = \sum_{i=1}^{v} 2n_F g_i^2/\hbar\omega_i$ where $n_F = (\pi\sqrt{2}t)^{-1}$ is the density of states per molecule per spin in the gapless band for the undistorted molecular stack. Alternatively, we can estimate the small-polaron binding energy $E_p = \sum_{i=1}^{v} g_i^2/\hbar\omega_i$. From the data in Tables II and III, we get representative values of $\lambda = 0.23$ and 0.37 and $E_p = 126$ meV and 168 meV for the TMTSF and TMTTF salts, respectively. The strength of the EMV interactions is therefore moderately strong with a larger dimensionless coupling constant for the TMTTF salts because of the narrower bandwidth, and hence larger n_F.

We should now turn to a discussion of the physical implications of our finding that the optical properties of the Bechgaard salts and of the related sulfur derivatives can be successfully accounted for only if one assumes a distribution function, Eq. (25), that precludes the dou-

ble occupancy of the electronic band states, namely the $\xi = 1$ scheme. This type of statistics applies both to the case of on-site electron correlation much larger than the bandwidth, $U \gg 4t$,[20] and to the occupancy of localized polaron or defect states by strongly correlated electrons.[67] Indeed, there is theoretical and experimental evidence that quasi-1D systems are particularly subject to localization phenomena caused by disorder,[68] polaronic effects,[69] and electron correlations.[70] The Hubbard model,[10] which is widely accepted as a means of describing theoretically various types of low-dimensional materials such as organic charge transfer conductors, conducting polymers, and high-T_c ceramic superconductors, presents strongly localized states in the $U \to \infty$ case.[70]

Disorder effects are expected to play a negligible role in the studied materials, which exhibit a high degree of crystalline perfection. Instead, electron correlations do play an important role in at least some of them, notably in the sulfur compounds.[13,39,71] It is therefore quite natural to assume that the on-site electron correlation U causes electron localization, in various degree, in all of the studied materials. Numerically exact extended Hubbard model calculations carried out for short chain segments (tetramers) have in fact shown[17,72] that, provided one focuses on the excitation spectrum up to energies of the order of U, it is not required that the on-site correlation energy be exceedingly larger than the one-electron bandwidth in order for the low-energy spectra to behave as if double occupancy was effectively excluded.

The above discussion leads one to propose a somewhat schematic picture of the $(TMTTF)_2X$ and $(TMTSF)_2X$ salts at room temperature as small-gap magnetic semiconductors. The gap is due to the anion potential, the stack dimerization, and, possibly, to the nearest-neighbor electron correlation. The Fermi level is shifted inside this gap because of the on-site correlation. However, this picture contrasts with direct evidence of the presence of a real Fermi surface coming, e.g., from low-temperature magnetotransport measurements.[73] One possible way to reconcile these views is to assume that on lowering the temperature the effect of the electron correlations changes dramatically.

Temperature changes may come into play in two possible ways: (i) because of the effects of the changing phonon population and (ii) by way of changes induced in the crystal structure due to anisotropic lattice contraction. An increasing phonon population with increasing temperature has the obvious consequence of reducing the carrier mean free path. It is not uncommon that the mean free path of organic molecular conductors is comparable to or even smaller than the intermolecular spacing. In effect, the increasing phonon population may play an important role regardless of the formation of small polarons and of the transition to incoherent hopping transport. In fact, the narrowing of the bandwidth, effective also in the polaron band regime,[74] increases as the temperature rises and could eventually lead to values of the U/t ratio large enough to split the band of doubly occupied states off that of singly occupied ones. It has also been pointed out[75] that in materials such as the $(TMTSF)_2X$ salts the polaron band narrowing is anisotropic; more precisely, it is such as to increase the 1D character of the band structure. It is worth noting that the discrepancy between the values of the transfer integrals we have obtained and those estimated from quantum-mechanical calculations employing double-ζ basis functions may originate in the inability of the latter to account for the polaron effects.

For some of the studied materials, x-ray scattering investigations[52,76] provide direct information on the effects of temperature on the structural properties. On cooling, a lattice contraction occurs mainly along the transverse **b** direction while the amplitude of the stack dimerization decreases. Correspondingly, the band structure tends to change progressively from quasi-1D to anisotropic 2D and the dimerization gap narrows. On account of the narrowness of this gap, particularly in the TMTSF salts, a direct consequence would be the transition from a 1D semiconductor to a 2D semimetal. In addition, an increased effectiveness of the screening of the Coulomb repulsions could reduce their importance and make the double occupancy of the electronic states increasingly allowed, eventually leading to a metallic structure. The above-mentioned anisotropic polaron band narrowing could enhance the temperature effects by adding its contribution to that of the structural changes.

VI. CONCLUSIONS

A systematic analysis of the optical properties of several members of the family of the Bechgaard salts $(TMTSF)_2X$, and their sulfur analogs $(TMTTF)_2X$, has allowed us to obtain a wealth of information on the electronic structure and interactions in these organic CT conductors. The approach adopted in this paper has been rather unusual in the comprehensive character of the data analysis. Such analysis has achieved the aim of accounting simultaneously for all the complex structures of the reflectance and conductivity spectra in a wide frequency range from the far to the near infrared. Furthermore, the variation of a limited number of model parameters, guided by the known crystal structural properties, has allowed us to reproduce the spectral changes observed among different members of the series.

The electronic structure of the studied compounds has been modeled as a 1D split tight-binding band characterized by a transfer integral t and by a dimerization gap Δ_b. An essential prerequisite to succeed in reproducing the observed spectral features has been to exclude the double occupancy of the band states so that the Fermi level shifts inside the dimerization gap. As a result, the electronic properties of the $(TMTSF)_2X$ and $(TMTTF)_2X$ salts at room temperature resemble those of 1D narrow-gap semiconductors with gap amplitudes ranging from 5% to 9% of the total bandwidth in the selenium compounds and from 12% to 24% in the sulfur ones. The smallest gap amplitudes amount to just a few k_BT at room temperature, so that the *metallic* character of the Bechgaard salts can be easily accounted for in terms of a comparatively large concentration of thermally excited carriers.

The estimated values of the parameters t and Δ_b fol-

low closely the changes in the structural properties of the studied materials, the former being related to the average interplanar spacing between molecules along the stacks, the latter to the structural dimerization Δd. The transfer integrals t assume effective values which account for polaron band narrowing effects as well as for a possible renormalization due to the finite values of the electron correlations.

Knowing the amplitude Δd of the structural dimerization and assuming a sensible value for the frequency of the phonon mode associated with the dimerization, it has been possible to clear up the relative roles of the EIP coupling and of the static potential in driving the formation of the b–CDW and the opening of the gap. It turns out that in all the studied compounds the key role is played by the static potential, so that the dimerization of the organic stacks is appropriately described as a structural effect caused by the commensurate inorganic anion sublattice rather than by a phonon-induced Peierls instability. By exploiting the same self-consistency argument, we have also been able to get hints on the range of values to be assigned to the EIP coupling constant $(\partial t/\partial u)_0$. It should be emphasized, however, that this is by no means a direct experimental estimate of this type of coupling, which is still one of the worse-known features of these materials and of organic CT conductors in general.

The deviations from a simple Drude behavior, observed to various extents in the spectra of the studied materials, have played a pivotal role in our analysis and in allowing us to draw the above conclusions. Among those deviations possibly the most important is the presence of vibronic structures induced by the coupling of the conduction electrons with the intramolecular vibrational modes of TMTSF or TMTTF. The frequency location, the amplitude, and the shape of these spectral features are determined by the electronic parameters t and Δ_b and by the EMV coupling constants g_i. It has been thereby possible to evaluate these last constants with a greater degree of reliability than in previous attempts. This is due to the fact that a single set of values has allowed us to reproduce the vibronic features in the whole series of Bechgaard salts despite the changing structural and electronic properties. A similar result has been obtained also for the sulfur analogs $(TMTTF)_2X$. Keeping in mind the expected similarity of the EMV coupling in a number of molecular structures derived from TTF, including BEDT-TTF, we have recently used the information obtained with the present work to try and assess the role of phonons in establishing the superconductivity in organic CT crystals as well as to predict the magnitude of the isotopic effect on the critical temperature.[77]

We finally recall that the overall picture of the $(TMTSF)_2X$ and $(TMTTF)_2X$ salts as quasi-1D strongly correlated semiconductors with narrow or very narrow gaps is suggested to hold only in the high-temperature range. An increased dimensionality (or reduced anisotropy) at lower temperature induced by changes in the structural properties and in the phonon populations may cause important changes in the electronic properties. Spectroscopic studies to probe this possibility and complement those reported in the present paper are presently under way in our laboratory.

ACKNOWLEDGMENTS

Financial support by the Italian National Research Council (CNR) and by the Ministry of the University and Scientific and Technological Research is acknowledged. This work was developed under the "Progetto Finalizzato Materiali Speciali per Tecnologie Avanzate" of the CNR.

[1] *Proceedings of the International Conference on Science and Technology of Synthetic Metals, Göteborg, Sweden, 1992* [Synth. Met. **55-57**, 1 (1993)].
[2] S. Kagoshima, H. Nagaswa, and T. Sambongi, *One-Dimensional Conductors* (Springer-Verlag, Berlin, 1988).
[3] T. Ishiguro and K. Yamaji, *Organic Superconductors* (Springer-Verlag, Berlin, 1990).
[4] D. Jérome and H. J. Schulz, Adv. Phys. **31**, 299 (1982).
[5] R. E. Peierls, *Quantum Theory of Solids* (Oxford University Press, Oxford, 1955), p. 108.
[6] D. Jérome, A. Mazaud, M.Ribaud, and K. Bechgaard, J. Phys. (Paris) Lett. **41**, L95 (1980).
[7] R. Bozio and C. Pecile, in *Spectroscopy of Advanced Materials*, edited by R. J. H. Clark and R. E. Hester (John Wiley & Sons, Chichester, 1991), p. 1.
[8] J. B. Torrance, B. A. Scott, B. Welber, F. B. Kaufman, and P. E. Seiden, Phys. Rev. B **19**, 730 (1979).
[9] C. S. Jacobsen, J. Phys. C **19**, 5643 (1986).
[10] J. Hubbard, Proc. R. Soc. London Ser. A **276**, 238 (1963); **277**, 237 (1964); **281**, 401 (1964); **285**, 542 (1965).
[11] J. Hubbard, Phys. Rev. B **17**, 494 (1978).
[12] S. Mazumdar and A. N. Bloch, Phys. Rev. Lett. **50**, 207 (1983); S. Mazumdar and S. N. Dixit, Phys. Rev. B **34**, 3683 (1986).
[13] R. Bozio, M. Meneghetti, and C. Pecile, J. Chem. Phys. **76**, 5785 (1982).
[14] R. Bozio, M. Meneghetti, and C. Pecile, Phys. Rev. B **36**, 7795 (1987).
[15] R. Bozio, M. Meneghetti, C. Pecile, and F. Maran, Synth. Met. **19**, 309 (1987); **20**, 393 (1987).
[16] R. Bozio, M. Meneghetti, D. Pedron, and C. Pecile, Synth. Met. **27**, B129 (1988).
[17] R. Bozio, M. Meneghetti, D. Pedron, and C. Pecile, in *Lower-Dimensional Systems and Molecular Devices*, edited by R. M. Metzger, P. Day, and G. Papavassiliou (Plenum, New York, 1991), p. 129.
[18] R. Bozio, D. Pedron, M. Meneghetti, and C. Pecile, Synth. Met. **42**, 1653 (1991).
[19] A fruitful recent approach to this problem considers ring-shaped molecular clusters. See, e.g., E. Y. Loh and D. K. Campbell, Synth. Met. **27**, A499 (1988); M. Meneghetti and C. Pecile, Phys. Rev. B **42**, 1605 (1990); M. Meneghetti, *ibid.* **44**, 8554 (1991); **47**, 13 151 (1993).
[20] J. F. Kwak and G. Beni, Phys. Rev. B **13**, 652 (1976).
[21] F. Wooten, *Optical Properties of Solids* (Academic, New York, 1972).

[22]C. C. Homes and J. E. Eldridge, Phys. Rev. B **42**, 9522 (1990).
[23]J. E. Eldridge and C. C. Homes, Phys. Rev. B **43**, 13 971 (1991).
[24]M. Meneghetti, R. Bozio, I. Zanon, C. Pecile, C. Ricotta, and M. Zanetti, J. Chem. Phys. **80**, 6210 (1984).
[25]K. Bechgaard, K. Carneiro, F. B. Rasmussen, M. Olsen, G. Rindorf, C. S. Jacobsen, H. J. Pedersen, and J. C. Scott, J. Am. Chem. Soc. **103**, 2440 (1981).
[26]K. Kikuchi, I. Ikemoto, K. Yakushi, H. Kuroda, and K. Kobayashi, Solid State Commun. **42**, 443 (1982).
[27]R. L. Musselman and B. M. Wolfe, Solid State Commun. **63**, 595 (1987).
[28]C. S. Jacobsen, D. B. Tanner, and K. Bechgaard, Phys. Rev. B **28**, 7019 (1983).
[29]K. Yakushi, S. Aratani, K. Kikuchi, H. Tajina, and H. Kuroda, Bull. Chem. Soc. Jpn. **59**, 363 (1986).
[30]M. Born and E. Wolf, *Principles of Optics* (Pergamon, Oxford, 1964).
[31]J. E. Eldridge and C. C. Homes, Infrared Phys. **29**, 143 (1989); C. C. Homes, Ph.D. thesis, University of British Columbia, 1990.
[32]U. Fano, Phys. Rev. **124**, 1866 (1961).
[33]G. Rindorf, H. Soling, and N. Thorup, Acta Crystallogr. Sect. B **38**, 2805 (1982).
[34]N. Thorup, G. Rindorf, H. Soling, and K. Bechgaard, Acta Crystallogr. Sect. B **37**, 1236 (1981).
[35]H. Kobayashi, A. Kobayashi, G. Saito, and H. Inokuchi, Chem. Lett. **1982**, 245.
[36]J. L. Galigné, B. Liautard, S. Peytavin, G. Brun, J. M. Fabre, E. Torreilles, and L. Giral, Acta Crystallogr. Sect. B **43**, 1453 (1982).
[37]B. Liautard, S. Peytavin, G. Brun, and M. Maurin, J. Phys. (Paris) **43**, 1453 (1982).
[38]S. Flandrois, C. Coulon, P. Delhaes, D. Chassen, C. Hauw, J. Gaultier, J. M. Fabre, and L. Giral, Mol. Cryst. Liq. Cryst. **79**, 307 (1982).
[39]D. Jérome, F. Creuzet, and C. Bourbonnais, Phys. Scr. **T27**, 130 (1989).
[40]M. J. Rice, Solid State Commun. **31**, 93 (1979).
[41]M. J. Rice, Phys. Rev. Lett. **37**, 36 (1976).
[42]R. Bozio and C. Pecile, in *The Physics and Chemistry of Low Dimensional Solids*, edited by L. Alcaser (Reidel, Dordrecht, 1980), p. 165.
[43]E. M. Conwell, Phys. Rev. B **22**, 1761 (1980).
[44]E. M. Conwell, Phys. Rev. B **18**, 1818 (1978).
[45]T. Holstein, Phys. Rev. **96**, 535 (1954).
[46]P. B. Allen, Phys. Rev. B **3**, 305 (1971).
[47]R. R. Joyce and P. L. Richards, Phys. Rev. Lett. **24**, 1007 (1970).
[48]We have verified that negligible Holstein's effects are predicted at room temperature for systems with total dimensionless EMV coupling constant $\lambda < 1$. Following the work of Allen (Ref. 46), we have calculated the room-temperature optical conductivity for a quarter-filled regular chain using our estimated TMTSF and TMTTF EMV coupling constants. The calculated optical conductivity spectra do not deviate appreciably from the regular Drude behavior.
[49]M. Krauzman, H. Poulet, and R. M. Pick, Phys. Rev. B **33**, 99 (1986).
[50]C. C. Homes and J. E. Eldridge, Phys. Rev. B **40**, 6138 (1989).
[51]J. Breitenstein, Ph.D. thesis, Université Paris VII, 1988.
[52]L. Ducasse, M. Abderrabba, J. Hoaran, M. Pesquer, B. Gallois, and J. Gaultier, J. Phys. C **19**, 3805 (1986).
[53]L. Ducasse and M. Abderrabba, Synth. Met. **19**, 327 (1987).
[54]P. M. Grant, J. Phys. (Paris) Colloq. **44**, C3–847 (1983).
[55]K. Bechgaard, K. Carneiro, M. Olsen, F. B. Rasmussen, and C. S. Jacobsen, Phys. Rev. Lett. **46**, 852 (1981).
[56]K. Bechgaard, C. S. Jacobsen, K. Mortensen, H. J. Pedersen, and N. Thorup, Solid State Commun. **33**, 1119 (1980).
[57]C. S. Jacobsen, H. J. Pedersen, K. Mortensen, G. Rindorf, N. Thorup, J. B. Torrance, and K. Bechgaard, J. Phys. C **15**, 2651 (1982).
[58]C. Coulon, P. Delhaes, S. Flandrois, R. Lagnier, E. Bonjour, and J. M. Fabre, J. Phys. (Paris) **43**, 1059 (1982).
[59]P. M. Grant, Phys. Rev. B **26**, 6888 (1982).
[60]E. M. Conwell, Chem. Scr. **17**, 69 (1981).
[61]N. O. Lipari, M. J. Rice, C. B. Duke, R. Bozio, A. Girlando, and C. Pecile, Int. Quantum Chem. Symp. **11**, 583 (1977).
[62]T. Mori, A. Kobayashi, Y. Sasaki, H. Kobayashi, G. Saito, and H. Inokuchi, Bull. Chem. Soc. Jpn. **57**, 627 (1984).
[63]M. E. Kozlov, K. I. Pokhodnia, and A. A. Yurchenko, Spectrochim. Acta, Part A **43**, 323 (1987).
[64]M. E. Kozlov, K. I. Pokhodnia, and A. A. Yurchenko, Spectrochim. Acta, Part A **45**, 437 (1989).
[65]M. Meneghetti, R. Bozio, and C. Pecile, J. Phys. (Paris) **47**, 1377 (1986).
[66]A. Painelli, A. Girlando, and C. Pecile, Solid State Commun. **52**, 801 (1984).
[67]I. A. Howard and E. M. Conwell, Phys. Rev. B **29**, 6879 (1984).
[68]R. E. Borland, Proc. R. Soc. Ser. A **274**, 529 (1963); A. A. Gogolin, Solid State Commun. **45**, 361 (1983), and references therein.
[69]D. Emin and T. Holstein, Phys. Rev. Lett. **36**, 323 (1976).
[70]E. H. Lieb and F. Y. Wu, Phys. Rev. Lett. **20**, 1445 (1968); J. Carmelo and D. Baeriswyl, Phys. Rev. B **37**, 7541 (1988).
[71]V. J. Emery, R. Bruinsma, and S. Barisic, Phys. Rev. Lett. **48** 1039 (1982).
[72]D. Pedron, R. Bozio, and C. Pecile (unpublished).
[73]J. F. Kwak, J. E. Schirber, R. L. Green, and E. M. Engler, Phys. Rev. Lett. **46**, 1296 (1981); K. Kajimura, H. Tokumoto, M. Tokumoto, K. Murata, T. Ukachi, H. Anzai, T. Ishiguro, and G. Saito, J. Phys. (Paris) Colloq. **44**, C3–1059 (1983).
[74]J. Appel, Solid State Phys. **21**, 193 (1968).
[75]A. A. Gogolin, Solid State Commun. **50**, 265 (1984).
[76]B. Gallois, J. Gaultier, C. Hauw, T. Lamcharfi, and A. Filhol, Acta Crystallogr. Sect. B **42**, 564 (1986); B. Gallois, J. Gaultier, T. Lamcharfi, F. Bechtel, A Filhol, L. Ducasse, and M. Abderrabba, Synth. Met. **19**, 321 (1987).
[77]D. Pedron, R. Bozio, M. Meneghetti, and C. Pecile, Mol. Cryst. Liq. Cryst. **234**, 161 (1993).